American Mineralogist, Volume 80, pages 1277–1285, 1995

Low-temperature phase transitions and the role of hydrogen bonds in lawsonite

Eugen Libowitzky, Thomas Armbruster
Laboratorium für chemische und mineralogische kristallographie der Universität Bern,
Freiestrasse 3, CH-3012 Bern, Switzerland

Abstract

The structure of lawsonite, $CaAl_2(Si_2O_7)(OH)_2 \cdot H_2O$, was refined from X-ray single-crystal data at six temperatures between 110 and 500 K. Two reversible phase transitions were found to occur: (1) Below 273(5) K the space group changes from *Cmcm* to *Pmcn*, accompanied by the loss of the *--m* mirror plane because of rotation of both H_2O and OH groups. This transition was monitored by the appearance of *C*-centering forbidden reflections ($h + k = 2n + 1$) and by nonlinear changes of cell constants and optical birefringence values vs. temperature. (2) Below 155(5) K the space group symmetry is further reduced to $P2_1cn$, accompanied by the loss of the *m*-- mirror plane because of unidirectional shifts of the *x* coordinates of the H atoms of the H_2O and OH groups, thus resulting in a polar structure.

The driving force of both transitions is apparently the development of cooperative hydrogen bonds. At elevated temperatures the OH and H_2O groups are constrained by strong librations to occupy sites with high point symmetry. At low temperatures and reduced thermal vibration the H atoms are allowed to shift towards neighboring O atoms, building up strong hydrogen bonds. Consequently, the H_2O and OH groups are shifted off their highly symmetric positions in an ordered fashion, thus lowering the space group symmetry in two steps.

The present structural data allow reinterpretation of previously published, low-temperature, infrared-spectroscopic and thermodynamic measurements on lawsonite.

Introduction

Lawsonite, $CaAl_2(Si_2O_7)(OH)_2 \cdot H_2O$, which usually occurs in high-pressure, low-temperature metamorphic environments, contains both discrete OH groups and H_2O molecules. The structure was first solved by Wickman (1947) in space group $C222_1$ and was later refined by Ruminova and Skipetrova (1959), who determined that the space group was *Ccmm*. Pabst (1959), Davis and Pabst (1960), Ruminova and Belov (1960), and Pabst (1961) resolved the space group discrepancy and confirmed the space group *Ccmm*. Baur (1978) also refined the structure of lawsonite and roughly located the H atoms by means of geometric considerations and electrostatic energy calculations. His data are in good agreement with the IR measurements of Labotka and Rossman (1974), who determined the orientation of the OH vectors in lawsonite. Only recently, a new mineral of the lawsonite type [hennomartinite, $SrMn_2(Si_2O_7)(OH)_2 \cdot H_2O$] was described by Armbruster et al. (1992, 1993). However, because of the presence of heavy elements it was not possible to locate the positions of the H atoms.

Lawsonite was reinvestigated at different temperatures for the following reasons: (1) Direct determination of the H positions (thus confirming or revising the previous papers on lawsonite) could be expected from a high-quality X-ray data set; (2) thermodynamic data of Perkins et al. (1980) showed two anomalies at about 130 and 273 K, which were attributed to the influence of fluid inclusions, even though a previous paper on lawsonite by King and Weller (1961) had reported similar anomalies; (3) a preliminary 110 K data set could not be satisfactorily refined in space group *Cmcm*, thus suggesting a phase transition; (4) low-temperature (78 K), infrared spectroscopic measurements by Labotka and Rossman (1974) showed two sharp absorption bands for the OH-stretching fundamental of the OH group in lawsonite. This splitting of energy, tentatively explained by reduced site symmetry, could not be reconciled with the unique OH vector direction in lawsonite by the present authors.

Unfortunately, the designation of the crystallographic axes of lawsonite has not been described consistently in the literature. In this study, the axes are defined as $a = 5.85$, $b = 8.79$, and $c = 13.13$ Å, and the space group is *Cmcm* (at room temperature).

Experimental procedure

Several well-shaped crystals of lawsonite up to 8 mm in size from Reed Ranch, Tiburon Peninsula, California, were used for the present investigation. They were almost clear and colorless with a light bluish tint, probably caused by traces of Fe and Ti [for a microprobe analysis refer to Baur (1978)]. In our preliminary investigation, fragments

0003–004X/95/1112–1277$02.00

TABLE 1. Experimental parameters of the lawsonite refinements between 110 and 500 K

T (±5) (K)	110	155	233	295	410	500
Space group	$P2_1cn$*	$Pmcn$*	$Pmcn$*	$Cmcm$	$Cmcm$	$Cmcm$
a (±0.001) (Å)	5.855	5.853	5.852	5.847	5.851	5.857
b (±0.001) (Å)	8.762	8.766	8.777	8.790	8.799	8.810
c (±0.001) (Å)	13.094	13.100	13.113	13.128	13.136	13.150
N_{refl}	8030	4831	2341	2057	3787	2008
N_{unique}	1836	1670	1280	967	971	969
N_{param}	147	103	103	52	52	52
R_{int} (%)	1.1	1.1	1.0	0.9	1.3	1.3
R (%)	2.3	2.5	1.9	1.6	1.7	1.8
R_w (%)	2.5	2.5	2.3	2.3	2.4	2.5
Goof	1.60	1.45	1.49	1.65	1.74	1.68
Resid. (e^-/Å^3)	0.5	0.7	0.5	<0.5	<0.5	<0.5

Note: $R = \Sigma \| F_{obs}| - |F_{calc}\| / \Sigma |F_{obs}|$, $R_w = [\Sigma w(|F_{obs}| - |F_{calc}|)^2 / \Sigma w|F_{obs}|^2]^{1/2}$, Goof = $[\Sigma w(|F_{obs}| - |F_{calc}|)^2/(N_{refl} - N_{param})]^{1/2}$.
* Shift in origin of (¼, ¼, 0).

of these crystals were checked by the X-ray precession method (Mo$K\alpha$ radiation) for twinning, systematic absences, and general sample quality. The orientation of the optical indicatrix with respect to the morphology and cleavage as given by Tröger (1982) ($X \parallel c$, $Y \parallel a$, $Z \parallel b$) was confirmed. According to our definition of the axes, the optical orientation is $X \parallel a$, $Y \parallel b$, $Z \parallel c$; hence, the plane of the optical axes is parallel to (010). The shape of the tabular crystals is defined by the pinacoid (001) and the prism (110). These two planes also define the directions of cleavage, which are excellent and good, respectively.

A thermogravimetric analysis of lawsonite powder showed that the material is stable up to ~850 K, above which it dehydrates. The diffuse X-ray pattern of the completely dehydrated experimental product could not be reconciled with the pattern of any known Ca-Al-Si-O compound.

X-ray investigations

A colorless, gem-quality, cube-shaped fragment of lawsonite measuring 0.25 × 0.25 × 0.25 mm was mounted on a silica-glass needle using a high-temperature–resistant epoxy resin. This single crystal was used for the collection of all X-ray data sets in the range of 110–500 K.

X-ray intensities were measured on a CAD4 Enraf-Nonius diffractometer using graphite monochromatized Mo$K\alpha$ radiation. Data were collected up to $\theta = 40°$ using the 1.5° ω-scan mode. Additional experimental conditions are summarized in Table 1. During the high-temperature measurements at 410(20) and 500(5) K the crystal was heated by a regulated (±5 K) hot-air blower. In the low-temperature experiments at 110(5), 155(5), and 233(5) K a conventional liquid nitrogen cooling device with an accuracy of ±2 K was used. The exact temperatures were checked after each experiment using a specially designed goniometer head with a thermocouple mounted at the crystal position.

A ψ-scan check of selected reflections did not show significant variations of intensity; hence, absorption corrections were not applied. Data reduction, including background and Lorentz-polarization corrections, was performed with the SDP system (Enraf-Nonius, 1983). The program SHELXTL (Siemens, 1990), with neutral atom-scattering factors, was used for the structure refinements. Because of the excellent quality of the data it was possible to refine isotropic displacement parameters (B) of the H atoms. All other atoms were refined with anisotropic displacement factors (U_{ij}).

To obtain additional information about the behavior of the phase transitions, lattice constants were refined from 14 reflections ($18° < \theta < 30°$) at 17 different temperatures between 110 and 500 K.

Optical investigations

Two crystal fragments, 2–3 mm in size, were oriented parallel to (001) on the basis of morphology and mounted on a self-constructed crystal grinder. They were ground with SiC abrasive paper and polished on both sides with γ-Al_2O_3. The final thickness of the two crystal slabs was 150(1) μm.

The values of birefringence (retardation, $\Delta_{xy} = n_y - n_x$) vs. temperature (90–570 K) were measured on a Leitz microscope equipped with a LINKAM THMS 600 heating and cooling stage (accuracy ±1K) and a Leitz narrow-band interference filter. The crystal slabs were adjusted to show maximum interference colors under crossed polarizers (45° position). They were heated and cooled in steps of 10 K (or less). Using the interference filter, the exact wavelength of extinction was determined at each temperature. This wavelength corresponds to the path difference of the two rays with different polarization directions [parallel X and Y in (001) slabs]. In a final step, after correcting for sample thickness and the order of extinction (third and fourth order in this case), the birefringence values (Δ_{xy}) were calculated. Because the wavelength dispersion of the birefringence influences the results obtained by this method, the refractive indices parallel to X and Y were determined for various wavelengths using the immersion technique.

RESULTS

Lawsonite, *Cmcm* structure

The final atomic positional parameters for the refinement of lawsonite in space group $Cmcm$ (295, 410, and

TABLE 2. Atomic positional parameters of lawsonite, *Cmcm*, at 295, 410, and 500 K

Atom	T (K)	x	y	z	B_{eq}
Ca	295	0	0.33321(3)	0.25	0.694(4)
	410	0	0.33330(3)	0.25	0.866(4)
	500	0	0.33317(4)	0.25	1.176(4)
Al	295	0.25	0.25	0	0.341(3)
	410	0.25	0.25	0	0.422(3)
	500	0.25	0.25	0	0.568(4)
Si	295	0	0.98043(3)	0.13300(2)	0.348(3)
	410	0	0.98045(3)	0.13297(1)	0.408(3)
	500	0	0.98025(3)	0.13294(2)	0.525(4)
O1	295	0	0.0496(1)	0.25	0.64(1)
	410	0	0.0492(1)	0.25	0.76(1)
	500	0	0.0485(1)	0.25	0.99(1)
O2	295	0.27263(7)	0.37884(5)	0.11693(3)	0.583(5)
	410	0.27274(6)	0.37907(5)	0.11683(3)	0.684(5)
	500	0.27290(7)	0.37930(6)	0.11678(3)	0.860(6)
O3	295	0	0.13758(7)	0.06497(4)	0.470(7)
	410	0	0.13763(7)	0.06521(4)	0.561(7)
	500	0	0.13750(8)	0.06561(5)	0.738(8)
O4	295	0	0.63922(8)	0.04793(5)	0.645(8)
	410	0	0.63952(8)	0.04797(4)	0.729(8)
	500	0	0.63971(9)	0.04781(5)	0.900(9)
O5	295	0	0.6093(2)	0.25	1.56(2)
	410	0	0.6097(2)	0.25	1.91(2)
	500	0	0.6103(2)	0.25	2.47(3)
Hw	295	0	0.660(2)	0.199(2)	3.9(6)*
	410	0	0.661(2)	0.199(2)	4.1(6)*
	500	0	0.659(2)	0.198(2)	3.6(6)*
Hh	295	0	0.559(3)	0.054(2)	7.1(8)*
	410	0	0.563(3)	0.056(2)	6.6(8)*
	500	0	0.565(4)	0.045(2)	7.7(9)*

* Refined isotropically.

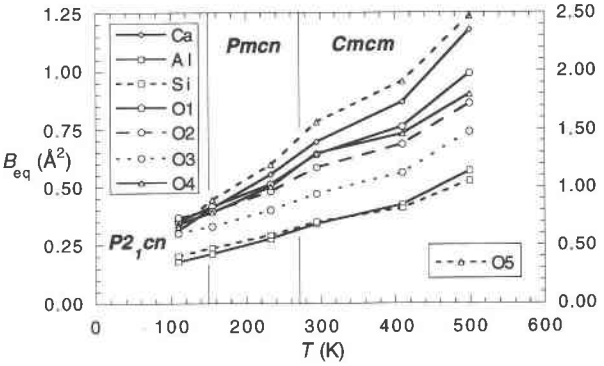

Fig. 1. Plot of B_{eq} vs. temperature.

500 K) are summarized in Table 2. Observed and calculated structure factors are given in Table 3, and anisotropic displacement factors are presented in Table 4.[1] Between 295 and 500 K the values of the fractional coordinates vary only within 3σ (standard deviation), and the isotropic temperature factors, B_{eq}, increase by the factor of 1.5 as indicated in Figure 1 for the whole temperature range. Except for the positions of the H atoms, the coordinates are in excellent agreement with those determined by Baur (1978). The H atoms, which were located in the present study by difference-Fourier syntheses and subsequent refinement, are located between the experimentally determined and geometrically (electrostatically) reasonable H positions of Baur (1978).

A projection of the lawsonite structure at 295 K parallel to [100] is presented in Figure 2. The structure consists of rods of edge-sharing AlO_6 octahedra that run parallel to [100] and are interconnected by Si_2O_7 groups. The remaining interstices of the framework are occupied by Ca, an H_2O molecule (O5, 2 × Hw), and an OH site (O4, Hh), which has twice the multiplicity of O5 (two OH groups p.f.u.). Selected interatomic distances and angles relating to the H_2O molecule and the OH group are given in Table 5.

The H_2O molecule occupies a special position with site symmetry $m2m$, the symmetry of a single, free H_2O molecule. The O5-Hw distances (0.80–0.81 Å) are shorter than those in a free H_2O molecule (approximately 0.98 Å). However, because X-ray methods locate electron densities rather than nuclei of atoms, these values are representative of the delocalized H electron and are in quite good agreement with O-H distances from other X-ray investigations (Lager et al., 1987). The H-O-H angle (112–116°), however, is larger than the one observed for a free H_2O molecule (104.5°). This might be caused by the attractive power of two additional hydrogen bonds to O4 atoms (1.98–2.00 Å) or by the librational motion of the H_2O molecule within the (100) plane. Proton NMR, sin-

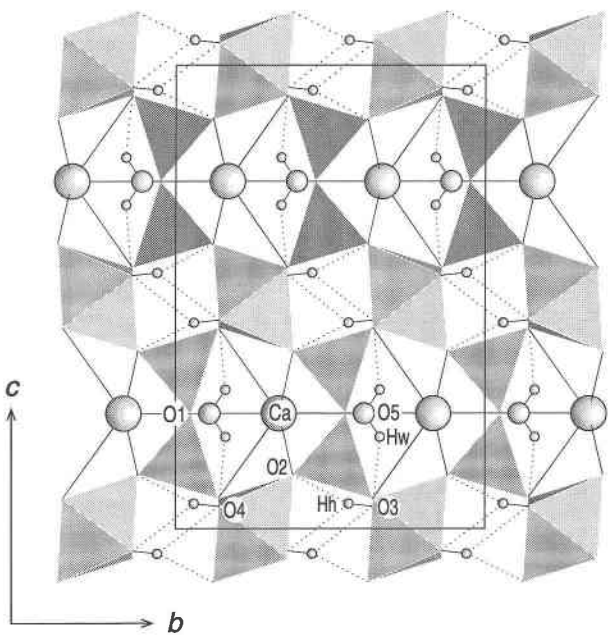

Fig. 2. The *Cmcm* structure of lawsonite at 295 K. Projection along [100]. The edge-sharing AlO_6 octahedra form rods parallel to [100] that are interconnected by Si_2O_7 groups. The interstices of the framework are occupied by Ca atoms (large spheres), H_2O molecules (O5, medium spheres), and the H atoms (small spheres) of the OH groups. Dotted lines represent O···H distances between 1.9 and 2.5 Å.

[1] A copy of Tables 3 and 4 may be ordered as Document AM-95-600 from the Business Office, Mineralogical Society of America, 1015 Eighteenth Street NW, Suite 601, Washington, DC 20036, U.S.A. Please remit $5.00 in advance for the microfiche.

Table 5. Selected interatomic distances (Å) and angles (°) in lawsonite at temperatures between 110 and 500 K

T (K)	110	155	233	295	410	500
O5-Hw	0.89(2)	0.85(2)	0.88(3)	0.80(2)	0.80(2)	0.81(2)
O5-Hwa	0.85(3)	0.79(3)	0.79(3)	equiv.	equiv.	equiv.
Hw-O5-Hwa	106(2)	110(2)	108(3)	112(3)	112(3)	116(3)
Ca-O5-Hw	108(1)	111(1)	113(2)	124(2)	124(2)	122(2)
Ca-O5-Hwa	145(2)	139(2)	139(2)	equiv.	equiv.	equiv.
Hw···O4	1.74(2)	1.78(2)	1.78(3)	1.99(2)	2.00(2)	1.98(2)
Hwa···O4a	2.38(3)	2.29(3)	2.26(3)	equiv.	equiv.	equiv.
Hwa···O2	2.33(3)	2.48(2)	2.50(2)	2.57(2)	2.58(2)	2.58(2)
O4-Hh	0.90(2)	0.90(3)	0.77(4)	0.71(3)	0.68(3)	0.66(3)
O4a-Hha	0.82(3)	0.80(3)	0.72(4)	equiv.	equiv.	equiv.
Hh···O4a	1.81(2)	1.82(3)	1.98(4)	2.20(3)	2.25(3)	2.17(3)
Hh···O2	2.39(4)	2.45(2)	2.50(3)	2.39(2)	2.41(2)	2.48(2)
Hha···O2a	2.18(3)	2.34(2)	2.37(3)	equiv.	equiv.	equiv.
Hha···O5	2.21(3)	2.21(3)	2.31(3)	2.61(3)	2.58(3)	2.73(3)
Si-O1-Sia	135.8(1)	135.9(1)	136.3(0)	136.8(0)	137.0(1)	137.3(1)
O1-Ca-O5	175.1(1)	178.5(0)	178.8(0)	180	180	180

Note: Values designated "equiv." are symmetrical equivalents of the values in the row above (because of the higher space group symmetry *Cmcm*). In space group *Cmcm* the atom sites marked with "a," e.g., Sia, are symmetrical equivalents of the original sites (without "a").

gle-crystal measurements on the 295 K *Cmcm* lawsonite phase suggest that the H atoms of the H_2O molecules and OH groups (see below) are dynamically (time averaged) disordered, thus oscillating between two equivalent sites similar to the ordered H positions in the low-temperature *Pmcn* structure (S. P. Gabuda and S. G. Kozlova, personal communication).

The H atoms of the OH groups are bound to O4 at a distance of 0.66–0.71 Å. As in the case of the H_2O molecule, these rather short bonds are a result of the delocalized H electron and may also indicate strong vibrational motion. Next-nearest neighbor O atoms are located at distances of 2.17–2.25 Å (O4) and 2.39–2.48 Å (O2). The O4-Hh vector and the O5-Hw vectors are parallel to (100), which was confirmed by polarized infrared spectroscopic investigations of Labotka and Rossman (1974).

The anisotropic displacement factors of O5 (the H_2O molecule) show a preferred elongation along [100] at all temperatures (U_{11}:U_{22}:U_{33} approximately 4:2:1). Nevertheless, a refinement with a split atom position and isotropic displacement factors [similar to that of hennomartinite (Armbruster et al., 1992, 1993)] did not significantly improve the *R* values reported in Table 1. The strongly anisotropic behavior of the O5 atom is explained by the next-neighbor environment, which forms a cavity elongated parallel to *a*. Thus, the anisotropic displacement factors reflect the interstice-constrained vibrational amplitudes of the singly coordinated (to Ca) O5 atom.

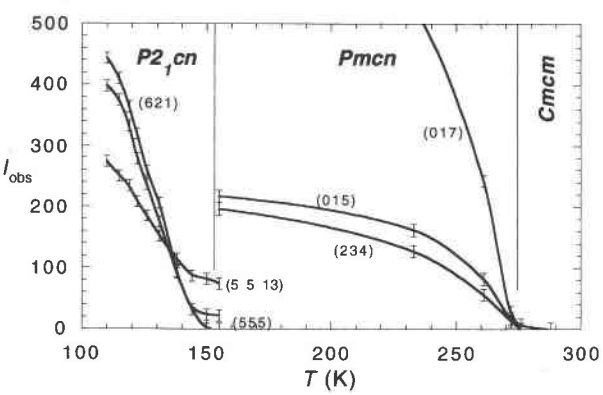

Fig. 3. Intensity (random units) vs. temperature plot of distinct X-ray reflections that were used to monitor the phase transitions in lawsonite.

Lawsonite, *Pmcn* structure

Below 273(5) K a series of additional reflections $h + k = 2n + 1$ were observed, which violate a C-centered cell. The three strongest of these reflections, 017, 015, and 234, were used to monitor the exact temperature of the phase transition (Fig. 3). These reflections were carefully checked at different ψ settings for any influence of multiple diffraction (*Umweganregung, Renningereffekt*). The correct determination of the space group also required additional ψ scans to filter out effects of multiple diffraction. Finally, almost all reflections violating the *-c-*, *--n,* and all 2_1 conditions could be rejected. Only the 0 0 17 reflection was present ($I > 15\sigma_I$) at all temperatures and ψ settings.

The atomic coordinates of the *Pmcn* lawsonite structure at 155 and 233 K are given in Table 6. Structure factors are listed in Table 3, and anisotropic displacement factors are presented in Table 4. In comparison with the *Cmcm* structure at room temperature, there seem to be no striking changes in the positions of the Ca, Al, Si, and O atoms. Only minor shifts (maximum 0.09 Å parallel to *c*) of the fractional coordinates are observed. However, as seen in Figure 4 and from the coordinates of the H atoms in Table 6, the phase transition is mainly characterized by the positions of the H atoms (maximum shifts of 0.4 Å parallel to *c*) and their next-neighbor interactions within the structure. The H_2O molecules rotate within the (100) plane, thus lowering the local *m*2*m* symmetry to *m*--. The OH groups (symmetrically related in the *Cmcm* structure) split into two different OH groups by rotation within the (100) plane.

Table 6. Atomic positional parameters of lawsonite, *Pmcn*, at 155 and 233 K

Atom	T(K)	x	y	z	B_{eq}
Ca	155	0	0.33211(2)	0.25098(1)	0.409(3)
	233	0	0.33250(3)	0.25075(2)	0.553(3)
Al	155	0.25	0.25	0	0.198(5)
	233	0.25	0.25	0	0.269(7)
Ala	155	0.25	0.25	0.5	0.226(5)
	233	0.25	0.25	0.5	0.283(8)
Si	155	0	0.98030(4)	0.13184(2)	0.232(4)
	233	0	0.98049(5)	0.13200(3)	0.285(6)
Sia	155	0	0.97837(4)	0.36563(2)	0.242(4)
	233	0	0.97895(5)	0.36589(2)	0.299(6)
O1	155	0	0.05004(9)	0.24891(5)	0.416(9)
	233	0	0.0498(1)	0.24919(7)	0.51(1)
O2	155	0.2756(1)	0.37319(7)	0.12012(3)	0.446(7)
	233	0.2749(2)	0.37470(9)	0.11942(5)	0.52(1)
O2a	155	0.27153(9)	0.37979(7)	0.38414(3)	0.343(7)
	233	0.2716(2)	0.38008(9)	0.38420(4)	0.45(1)
O3	155	0	0.1373(1)	0.06313(5)	0.34(1)
	233	0	0.1375(1)	0.06359(6)	0.39(2)
O3a	155	0	0.1355(1)	0.43421(4)	0.33(1)
	233	0	0.1360(1)	0.43420(6)	0.42(2)
O4	155	0	0.6402(1)	0.05104(5)	0.35(1)
	233	0	0.6406(1)	0.05084(7)	0.44(2)
O4a	155	0	0.6328(1)	0.45915(5)	0.43(1)
	233	0	0.6346(1)	0.45757(8)	0.57(2)
O5	155	0	0.6087(1)	0.24826(6)	0.89(1)
	233	0	0.6089(1)	0.24855(8)	1.19(2)
Hw	155	0	0.642(2)	0.187(1)	1.9(4)*
	233	0	0.647(3)	0.187(2)	3.4(7)*
Hwa	155	0	0.678(3)	0.287(2)	3.5(6)*
	233	0	0.677(3)	0.287(2)	3.3(7)*
Hh	155	0	0.541(3)	0.035(2)	3.6(5)*
	233	0	0.555(5)	0.038(3)	7.2(6)*
Hha	155	0	0.571(4)	0.415(2)	7.1(8)*
	233	0	0.571(5)	0.423(3)	9.7(13)*

* Refined isotropically.

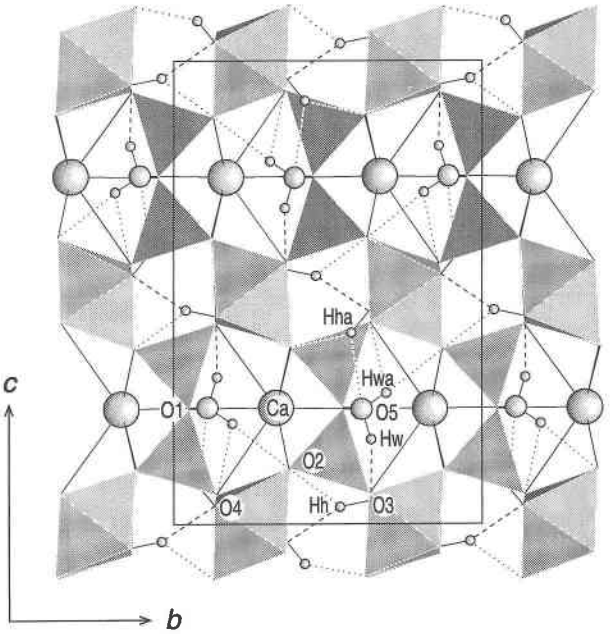

Fig. 4. The $P2_1cn$ structure of lawsonite at 110 K. In this projection the rotation of the H_2O molecules and the OH groups is almost the same as for the 155 and 233 K *Pmcn* structures, except that in the latter structures all OH vectors are aligned parallel to the (100) plane. In the 110 K structure the Hwa atoms deviate below and the Hha atoms above the (100) plane. Dashed lines represent strong hydrogen bonds, dotted lines indicate O···H bonds between 2.1 and 2.5 Å.

Table 5 summarizes the most important distances and angles around the H atoms. It is evident that all these rotations are caused by the tendency of the H atoms to form extensive hydrogen bond systems. The assumption of a transition mechanism related to minor shifts of the framework atoms must be rejected because a bond-valence analysis (Brese and O'Keeffe, 1991) did not show significant variations between the high- and low-temperature phases. Thus, the small shifts of the framework atoms seem to be caused by the rotations of the H_2O and OH groups. At 155(233) K the length of the hydrogen bond of the H_2O molecule (Hw···O4) is 1.78(1.78) Å. The respective O5-Hw distance is 0.85(0.88) Å, which is slightly longer than the O5-Hwa distance of 0.79(0.79) Å. This H atom is also linked to two O atoms at distances of 2.29(2.26) Å (O4) and 2.48(2.50) Å (O2). The rotation is best demonstrated by analysis of the Ca-O5-H angles. In the *Cmcm* structure, the two angles (124°) are constrained to be equal by the --*m* plane. They are split (111-113° and 139-139°) as the symmetry is lowered to *Pmcn*.

The length of the OH hydrogen bond (Hh···O4a) is 1.82 Å at 155 K and 1.98 Å at 233 K. The corresponding O4-Hh distances (0.90 and 0.77 Å) are slightly longer than the O-H distances of the Hha atoms (0.80 and 0.72 Å). The latter are also coordinated to O2a (2.34 and 2.37 Å) and to O5 (2.21 and 2.31 Å).

Lawsonite, $P2_1cn$ structure

Refinement of the *Pmcn* structure with the 110 K X-ray data set yielded unsatisfactory R values and poorly defined H positions, even though the systematic absences were the same as for the *Pmcn* data sets (at 155 and 233 K). A careful but unsuccessful refinement in space group $P\bar{1}$ showed that the structure lost the center of symmetry. Consequently, a refinement in space group $P2_1cn$ (which is the noncentrosymmetric subgroup of *Pmcn*) was performed and successfully converged to a final $R = 2.3\%$. The exact transition temperature was determined by monitoring three reflections that had shown the most striking differences between F_o and F_c in the unsuccessful *Pmcn* refinement. As seen in Figure 3, the 621, 55·13, and 555 reflections increase in intensity just below 150(5) K. The continuously negative slope of the three curves at 110 K indicates that the atom positions have not attained their final low-temperature configuration. This fact will be discussed later.

The final atomic positional parameters of the 110 K structure are given in Table 7, structure factors are listed in Table 3, and anisotropic displacement factors are presented in Table 4. A projection of the structure is shown in Figure 4. The major differences (except for minor changes up to 0.05 Å in the framework atoms) between the 155 and 110 K structure are once again related to the positions of the H atoms (maximum shifts of 0.25 Å par-

TABLE 7. Atomic positional parameters of lawsonite, $P2_1cn$, at 110 K

Atom	x	y	z	B_{eq}
Ca	0.0066(1)	0.33176(2)	0.25106(1)	0.311(3)
Al	0.25	0.24952(8)	−0.00036(6)	0.192(5)
Ala	0.2458(1)	0.25214(8)	0.50131(5)	0.162(5)
Si	−0.0031(1)	0.98003(4)	0.13181(2)	0.198(4)
Sia	−0.0010(1)	0.97795(4)	0.36558(2)	0.205(4)
O1	−0.0076(2)	0.0499(1)	0.24891(5)	0.35(1)
O2	0.2752(2)	0.3731(2)	0.1192(1)	0.367(5)*
O2a	0.2675(2)	0.3818(2)	0.38584(9)	0.367(5)*
O2b	−0.2763(2)	−0.3765(2)	−0.11797(9)	0.367(5)*
O2c	−0.2761(2)	−0.3719(2)	−0.37840(9)	0.367(5)*
O3	0.0024(2)	0.13682(9)	0.06297(5)	0.29(1)
O3a	−0.0011(2)	0.13475(9)	0.43428(5)	0.32(1)
O4	−0.0062(2)	0.6395(1)	0.05075(5)	0.31(1)
O4a	−0.0007(3)	0.6320(1)	0.45967(5)	0.38(1)
O5	−0.0130(3)	0.6094(1)	0.24811(6)	0.66(1)
Hw	−0.004(9)	0.640(2)	0.183(2)	2.8(5)**
Hwa	0.958(7)	0.689(3)	0.283(2)	3.4(6)**
Hh	0.008(8)	0.539(3)	0.037(2)	2.5(5)**
Hha	0.043(7)	0.576(3)	0.414(2)	5.4(8)**

* Refined with $U_{ij}(O2) = U_{ij}(O2a) = U_{ij}(O2b) = U_{ij}(O2c)$; $i = 1–3$.
** Refined isotropically.

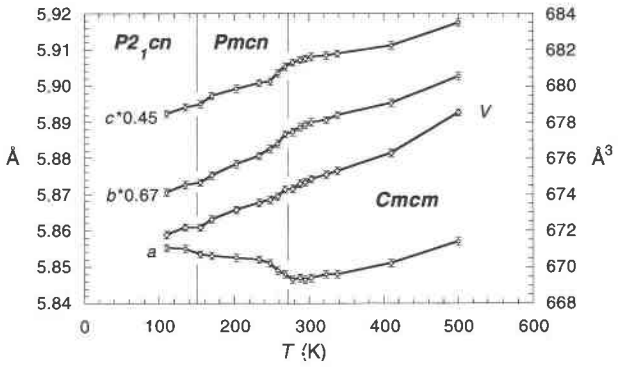

Fig. 5. Plot of unit-cell constants (*a, b, c*) and *V* of lawsonite vs. temperature. The *Cmcm-Pmcn* phase transition at 273 K is characterized by a minimum value of *a*, followed by a strong, anomalous increase of *a* with decreasing temperatures. Error bars represent $\pm 1\sigma$.

allel to *a*). Whereas the H atoms are on special positions (mirror plane *m*-- at $x = 0$) in the *Pmcn* structure, in the $P2_1cn$ structure the weakly bonded H atom of the H_2O molecule shifts below the former *Pmcn m*-plane (to $x = 0.958$), and the weakly bonded H atom of one OH group shifts off the zero level (to $x = 0.043$). Simultaneously, the longer O···H distances of the weakly bonded H atoms are shortened: Hwa···O4a at 2.38 Å is close to Hwa···O2 at 2.33 Å, and Hha···O2a at 2.18 Å comes close to Hha···O5 at 2.21 Å. The stronger hydrogen bonds are enhanced by shortening the distances to 1.74 Å (Hw···O4) and 1.81 Å (Hh···O4a). As can be seen from the Ca-O5-H angles, the H_2O molecule, now occupying a general position, is further rotated off the Ca-O5 line. Because of the decrease of the *x* coordinate of the Hwa atom the O atom of the H_2O molecule (O5) is also shifted below the zero level (to $x = -0.013$). The short O-H bonds (between 0.8 and 0.9 Å) behave quite similarly to those in the *Pmcn* structure.

Nonlinear changes of lattice constants and birefringence values

The lattice constants (*a, b, c*) and the cell volume (*V*) vs. temperature (110–500 K) are plotted in Figure 5. Although the unit-cell volume is quite linear (within estimated standard deviation), the unit-cell parameters show considerable deviations from linearity. The most dramatic changes occur in the values of *a*. Starting at 500 K the *a* values decrease smoothly from 5.857(1) to 5.847(1) Å at 278(5) K. At this temperature, representing the *Cmcm-Pmcn* transition, the value of *a* reaches its absolute minimum. Below this temperature the slope changes and the values of *a* increase to 5.852(1) Å at about 240 K. The slope remains negative up to the *a* value of 5.855(1) Å at 110 K. Because of the magnitude of the standard deviations of the lattice constants, the *Pmcn-*$P2_1cn$ transition cannot be fixed unambiguously. The *b* and *c* constants show similar nonlinear behavior.

The decrease in the *b* and *c* values together with the rather anomalous increase of *a* is easily explained from the structural changes at low temperatures. The rotation of the H_2O molecules and OH groups within the (100) plane, which is related to the enhancement of hydrogen bonds in (100), causes *b* and *c* to decrease sharply below 273 K (*Cmcm-Pmcn* phase transition). Because *V* decreases linearly, *a* must increase at temperatures below 273 K. The additional expansion of *a* below 155 K (*Pmcn-*$P2_1cn$ transition) is caused by the off-plane movement of the OH vectors of the OH and H_2O groups. However, the nonlinearities of the lattice constants observed at the transition temperatures are less pronounced in comparison with the increase of distinct X-ray reflections, as demonstrated in Figure 3.

The optical behavior, especially the nonlinear increase of the birefringence values with decreasing temperature, is intimately related to the anomalous changes in the lattice constants. A graph, plotting birefringence (retardation) values ($\Delta_{xy} = n_y - n_x$) vs. temperature in the range from 86 to 573 K is given in Figure 6. Starting at 573 K, the birefringence increases from 0.0100 to 0.0117 at 273(1) K, showing a concave-up slope. Down from the kink at the *Cmcm-Pmcn* transition point the birefringence continues with a steeper but concave-down slope to values as high as 0.0153 at 86 K. The *Pmcn-*$P2_1cn$ transition point may be interpreted from this curve to lie at ~120 K (visible by an insignificant, concave-up increase in the slope), but considering the estimated standard deviation this is not a conclusive argument.

The inconvenient break between the birefringence curves of the third- and fourth-order extinction is caused by the experimental procedure itself, which introduces the wavelength dispersion of the birefringence as another variable. Even if the effect has no influence on the shape of the curves, it produces a break at the expected junction of the two curves. This can be explained as follows: As-

suming that the birefringence at 600 nm equals that at 450 nm (at a given temperature), the third-order extinction at 600 nm should be the same as the fourth-order extinction at 450 nm, i.e., if $\Delta_{600} = \Delta_{450}$, then 3×600 nm $= \Delta_{600}$ equals $\Delta_{450} = 4 \times 450$ nm. Contrary to this theoretical assumption, we observe in the case of natural lawsonite that 3×600 nm $= \Delta_{600} < \Delta_{450} = 4 \times 450$ nm. Therefore, Δ at higher wavelengths must be smaller than Δ at short wavelengths. To further check the validity of this relationship, the refractive indices n_x and n_y were determined at room temperature with the immersion technique covering the wavelength region between 450 and 650 nm. The results, presented in the Figure 6 inset, clearly confirm that Δ_{xy} is indeed smaller at longer wavelengths and vice versa. The measured refractive indices also coincide (within estimated standard deviation) with the approximate values given by Tröger (1982) for white light. The slightly higher birefringence of the samples of this investigation (0.011 instead of 0.010) can be attributed to minor amounts of Fe and Ti, which are also likely to produce the light blue tint of the crystals.

The correlation between the changes in the lattice constants and the changes in the birefringence values can be explained by the fact that the enhanced hydrogen bonds, which cause the lattice to compress in the (100) plane and to relax by expansion along [100], considerably influence the electronic polarizations and, thus, the refractive indices along the principal optical directions. The hydrogen bonds that are enhanced below the 273 K transition point are all oriented in the (100) plane. Thus, the electronic polarizations (and consequently the refractive indices) along Y and Z increase. The expansion of the a lattice constant causes the electronic polarization to decrease along [100], thus leading to a decrease in the refractive index along X.

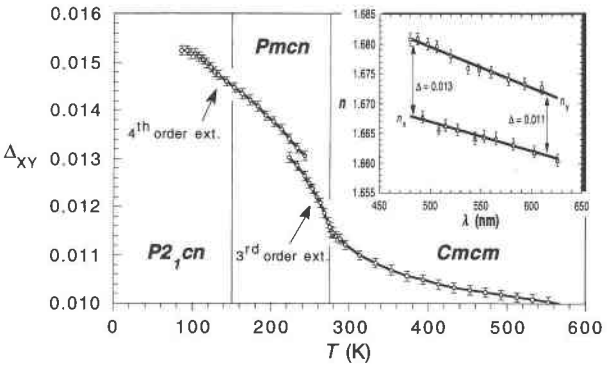

Fig. 6. Plot of birefringence (retardation) values (Δ_{xy}) of lawsonite vs. temperature. The *Cmcm-Pmcn* phase transition at 273 K is characterized by a kink in the slope of the curve, changing from concave-up at elevated temperatures to concave-down at low temperatures. The interruption between the third- and fourth-order extinction curves is caused by the wavelength dispersion of the birefringence values. This is shown in the small window, where the refractive indices n_x and n_y are plotted vs. wavelength. Error bars represent $\pm 1\sigma$.

Discussion

Displacive phase transitions are fairly common in solids. Recently described examples include quartz [low-quartz–high-quartz transition at 575 °C (Kihara, 1990)] and titanite, $CaTiSiO_5$ (Bismayer et al., 1992). The phase transition ($A2/a$ to $P2_1/a$) in titanite characterized by a collinear displacement of the heavy Ti atoms (in contrast to the displacement of only OH and H_2O groups in lawsonite at very low temperatures) occurs at elevated temperatures (496 K). The transition was determined by a nonlinearity in birefringence values identical to that observed in lawsonite. The change from concave-up to concave-down at the transition kink seems to be a typical feature of this type of transition (the birefringence values in titanite decrease with decreasing temperature, which is opposite to that in lawsonite). Similar to the present investigation, Bismayer et al. (1992) observed additional, A-centering forbidden X-ray reflections appearing just below the transition temperature, which show an almost identical intensity vs. temperature profile as that in lawsonite.

Both transitions in lawsonite fulfill the conditions of symmetry reduction leading to "maximal non-isomorphic" subgroups (according to Wilson, 1992): (1) *Pmcn* is a subgroup of *Cmcm* accompanied by the loss of the *--m* plane. As indicated by an unsuccessful refinement in space group *Pmcm,* the loss of the C centering is not the primary effect. Rather, it is a consequence of the loss of the mirror plane. As in the case of the $A2/a$-$P2_1/a$ phase transition in titanite (Bismayer et al., 1992), the *Cmcm-Pmcn* transition in lawsonite occurs within the same crystal class and can be classified as "antiferrodistortive" (Blinc and Zeks, 1974). (2) $P2_1cn$ is a subgroup of *Pmcn* associated with the loss of the *m--* symmetry plane. Thus, it is one of the noncentrosymmetric subgroups of *Pmcn.* It is interesting to note that in Figures 5 and 6 the *Pmcn*-$P2_1cn$ phase transition at 155 K is not as apparent as the transition at 273 K. One reason might be that the $P2_1cn$ structure at 110 K has not reached the final stage of development. This explanation is supported by Figure 3, which shows that the intensities of the new X-ray reflections still increase at 110 K. Another reason for the weak impact of the 155 K transition on physical constants might be that the strong hydrogen bonds have already formed during the 273 K transition, and that the 155 K shift of the H atoms below or above the pseudo-(100) *m* plane is only a minor adjusting motion. However, as demonstrated in Figure 3, the transition can be clearly monitored by the enhancement of distinct X-ray reflection intensities.

As mentioned in the introduction, evidence for the two phase transitions in lawsonite was observed by Perkins et al. (1980) and in a similar way by King and Weller (1961), although they were not aware of the fact. These authors measured the heat capacity of lawsonite from extremely low (5 K) to high temperatures (600 K) to calculate various thermodynamic constants. They noticed two anomalies (or rather nonlinearities) but attributed them to the fusion point of water and a transition point

of ice in aqueous inclusions. The thermodynamic data were finally obtained by smoothing out these anomalies. There is no evidence that this will dramatically influence the reliability of the high-temperature thermodynamic data because the phase transitions of lawsonite occur at temperatures that are not relevant for petrological systems. However, because the high-pressure behavior of minerals is often comparable to their low-temperature behavior (because both pressure and low temperatures lead to decreased cell volume, allowing for similar crystal-chemical effects), the data should be reconsidered to avoid uncertainties in thermodynamic calculations at elevated pressures. Obviously, this is the case for lawsonite, which represents an important constituent of high-pressure, low-temperature phase assemblages, e.g., blueschists.

Comparison of the X-ray results of this study and the IR spectroscopic results of Labotka and Rossman (1974) seems worth some discussion. The latter authors recorded polarized IR spectra of very thin, oriented lawsonite slabs, covering the OH-stretching and H_2O-bending region at room temperature as well as at 78 K. The results at room temperature prove that all OH vectors (of OH and H_2O groups) are oriented within the (100) plane [denoted according to the present setting; Labotka and Rossman (1974) used a different setting]. Unfortunately, at 78 K the polarized spectrum parallel to *a* is missing, thus we cannot compare our results [which should show a deviation from the (100) plane] with those from IR spectroscopy. The maximum absorption of the H_2O bending mode at room temperature (which is parallel to the twofold axis of the H_2O molecule) is parallel to *b*, which confirms the results of the present paper as well as that of the structure refinement of Baur (1978). The detailed orientation of the hydroxide OH vectors within the (100) plane is more difficult to determine. At room temperature, the spectra along [010] and [001] reveal an OH band that is almost equally absorbing, thus indicating that the OH vectors are mediating between the *b* and *c* axes. In contrast, results from the present structure refinement indicate an OH vector that is aligned almost parallel to *b* (Fig. 2). A similar OH direction was also obtained by Baur (1978). A possible explanation might be that the OH groups that, at room temperature, show weaker hydrogen bonding in comparison with the low-temperature structures oscillate about their positions, thus resulting in an OH vector that mediates between the *b* and *c* axes. Therefore, the refined Hh position of the present paper represents a diffuse center of thermal motion. This assumption is further supported by the isotropic displacement parameter of the H atoms: *B* of Hh is almost twice the *B* of Hw (Table 2).

The polarized IR spectra of lawsonite at 78 K from Labotka and Rossman (1974) show two sharp OH-stretching bands instead of one broad band at room temperature. In view of the present results these two peaks can be assigned to the two different OH positions in the $P2_1cn$ structure. Again, both OH bands indicate a vector that mediates between the [010] and [001] directions. Our results verify this only for the H atom Hha. The OH vector of the Hh atom is aligned almost parallel to *b*. A possible explanation is that the H atom is oscillating, similar to that in the room temperature structure. However, this seems improbable because the oscillation should be reduced as a result of the low temperature and the strong hydrogen bond to O4a. This explanation is also confirmed by the rather small *B* of Hh. A more reasonable explanation is that the 110 K structure determined in this investigation has not fully developed (as was discussed above). Thus, 110 and 78 K data cannot be directly compared. However, if we assume that the final atomic arrangement has developed at 78 K, the polarized IR spectra suggest that the Hh atom is further rotated until the OH vector is located in a 45° position between the *b* and *c* axes.

In the near future, a detailed, polarized IR study of lawsonite as well as a proton NMR investigation at different temperatures will be conducted to obtain additional information about these fascinating, hydrogen-coupled phase transitions.

Acknowledgments

The authors thank L. Diamond for the introduction to the cooling and heating stage. R. Giovannoli performed the thermogravimetric analysis of lawsonite. The sample NMBE A7331 was obtained from B. Hofmann, Museum of Natural History, Bern. S.P. Gabuda and S.G. Kozlova (Novosibirsk, Russia) provided the room temperature proton NMR data, which is gratefully acknowledged. The comments of G.A. Lager, B. Downs, and an anonymous referee helped to improve the quality of the manuscript. E.L. is indebted to the Schweizer Nationalfonds, which granted financial support.

References cited

Armbruster, T., Oberhänsli, R., and Bermanec, V. (1992) Crystal structure of $SrMn_2[Si_2O_7](OH)_2 \cdot H_2O$, a new mineral of the lawsonite type. European Journal of Mineralogy, 4, 17–22.

Armbruster, T., Oberhänsli, R., Bermanec, V., and Dixon, R. (1993) Hennomartinite and kornite, two new Mn^{3+} rich silicates from the Wessels Mine, Kalahari, South Africa. Schweizerische Mineralogische und Petrographische Mitteilungen, 73, 349–355.

Baur, W.H. (1978) Crystal structure refinement of lawsonite. American Mineralogist, 63, 311–315.

Bismayer, U., Schmahl, W., Schmidt, C., and Groat, L.A. (1992) Linear birefringence and X-ray diffraction studies of the structural phase transition in titanite, $CaTiSiO_5$. Physics and Chemistry of Minerals, 19, 260–266.

Blinc, R., and Zeks, B. (1974) Soft modes in ferroelectrics and antiferroelectrics, 317 p. North-Holland, Amsterdam, the Netherlands.

Brese, N.E., and O'Keeffe, M. (1991) Bond valence parameters for solids. Acta Crystallographia, B47, 192–197.

Davis, G.A., and Pabst, A. (1960) Lawsonite and pumpellyite in glaucophane schist, North Berkeley Hills, California, with notes on the X-ray crystallography of lawsonite. American Journal of Science, 258, 689–704.

Enraf-Nonius (1983) Structure determination package (SDP). Enraf-Nonius, Delft, the Netherlands.

Kihara, K. (1990) An X-ray study of the temperature dependence of the quartz structure. European Journal of Mineralogy, 2, 63–77.

King, E.G., and Weller, W.W. (1961) Low temperature heat capacities and entropies at 298.15°K of some sodium- and calciumaluminum silicates. U.S. Bureau of Mines Report Inv. 5855. Cited in Perkins et al. (1980).

Labotka, T.C., and Rossman, G.R. (1974) The infrared pleochroism of lawsonite: The orientation of the water and hydroxide groups. American Mineralogist, 59, 799–806.

Lager, G.A., Armbruster, T., and Faber, J. (1987) Neutron and X-ray diffraction study of hydrogarnet $Ca_3Al_2(O_4H_4)_3$. American Mineralogist, 72, 756–765.

Pabst, A. (1959) False symmetry, the Templeton effect, in lawsonite. Zeitschrift für Kristallographie, 112, 53–59.

——— (1961) Supplementary note on "False symmetry, the Templeton effect, in lawsonite." Zeitschrift für Kristallographie, 115, 307–309.

Perkins, D., Westrum, E.F., and Essene, E.J. (1980) The thermodynamic properties and phase relations of some minerals in the system CaO-Al_2O_3-SiO_2-H_2O. Geochimica et Cosmochimica Acta, 44, 61–84.

Ruminova, I.M., and Belov, N.V. (1960) False symmetry of lawsonite. Kristallografiya, 5, 215–217.

Ruminova, I.M., and Skipetrova, T.I. (1959) The crystal structure of lawsonite. Døklady Akademie Nauk SSSR, 124, 324–327.

Siemens (1990) SHELXTL PC 4.1. Siemens Analytical X-ray Instruments, Madison, Wisconsin.

Tröger, W.E. (1982) Optische Bestimmung der gesteinsbildenden Minerale (5th edition), 188 p. Schweizerbart, Stuttgart, Germany.

Wickman, F.E. (1947) The crystal structure of lawsonite, $CaAl_2(Si_2O_7)(OH)_2 \cdot H_2O$. Arkiv för Kemie Mineralogi och Geologi, 25A, 1–7.

Wilson, A.J.C., Ed. (1992) International tables for crystallography, vol. A, 878 p. Kluwer Academic, Dordrecht, the Netherlands.

Manuscript received November 12, 1994
Manuscript accepted July 7, 1995